

# Satellite Dynamics Toolbox Library: a tool to model multi-body space systems for robust control synthesis and analysis

Francesco Sanfedino\* Daniel Alazard\* Ervan Kassarian\*\*  
Franca Somers\*\*\*

\* ISAE-SUPAERO, Université de Toulouse, Toulouse, France

\*\* DyCSyT S.A.S, Toulouse, France

\*\*\* ONERA, The French Aerospace Lab, Toulouse, France

(emails:[francesco.sanfedino/daniel.alazard]@isae.fr,

ervan.kassarian@dycsy.com, franca.somers@onera.fr)

---

**Abstract:** The level of maturity reached by robust control theory techniques nowadays contributes to a considerable minimization of the development time of an end-to-end control design of a spacecraft system. The advantage offered by this framework is twofold: all system uncertainties can be included from the very beginning of the design process; the validation and verification (V&V) process is improved by fast detection of worst-case configurations that could escape to a classical sample-based Monte Carlo simulation campaign. Before proceeding to the control synthesis and analysis, a proper uncertain plant model has to be available in order to push these techniques to their limits of performance. In this spirit, the Satellite Dynamics Toolbox Library (SDTlib) offers many features to model a spacecraft system in a multi-body fashion on SIMULINK. Parametric models can be easily built in a Linear Fractional Transformation (LFT) form by including uncertainties and varying parameters with minimal number of repetitions. Uncertain Linear Time Invariant (LTI) and uncertain Linear Parameter-Varying (LPV) controllers can then be synthesized and analyzed in a straightforward way. The authors present in this article a tutorial, that can be downloaded at <https://nextcloud.isae.fr/index.php/s/XDFrfHntejHTmmp>, to show how to deal with an end-to-end robust design of a spacecraft mission and to provide to researchers a benchmark to test their own algorithms.

*Keywords:* Spacecraft dynamics, robust control, robustness analysis, verification and validation industrial process,  $\mu$ -analysis, probabilistic  $\mu$ -analysis

---

## 1. INTRODUCTION

End-to-end spacecraft control design in industry is a long process that starts with the modeling of the spacecraft dynamics and ends up with the V&V campaigns. This process is not sequential and several iterations are necessary before system certification occurs. The major difficulty consists in assuring that the system will behave correctly without loss of stability and performance in presence of many system uncertainties. The LFT framework, developed from the early eighties (Doyle (1982)), offers the possibility to design robust control laws in spite of parametric and dynamic uncertainties in the system and to analyze then the closed-loop stability and worst-case (WC) performance. In order to put in place these techniques, now available in the Robust Control Toolbox of MATLAB (Balas et al. (2021)), an LFT model of the plant has to be built. The number of uncertain/varying parameters' repetitions affects the efficiency of the synthesis/analysis algorithms and has to be kept minimal. The Satellite Dynamics Toolbox Library (SDTlib) (Alazard and Sanfedino (2020)), based on the Two-Input Two-Output Port (TITOP) theory (Alazard et al. (2015)), allows the user to build a multi-body flexible spacecraft in the LFT frame-

work by assembling of elementary blocks in SIMULINK. Simple bodies (rigid bodies, flexible beams, flexible plates), complex Finite Element Model (FEM) structures (that can be imported from NASTRAN analysis files), mechanisms (reaction wheels, solar array drive mechanisms) and other flexible dynamics (i.e. sloshing effects) are available in this library.

The main objective of this paper is to present a demo of a complete design process of an attitude control system (ACS) for a spacecraft mission by combining the SDTlib together with the features available in the Robust Control Toolbox, the SMAC library (Biannic et al. (2016)) and the STOWAT library (Thai et al. (2019)). This benchmark is destined to researchers and industrial actors who would like to be introduced to the proposed techniques and/or to test their own robust control/analysis algorithms. The results presented in this paper were run in MATLAB R2021b on a MacBook Pro 2 GHz Intel Core i5. In the following parts of the article, Section 2 will detail the spacecraft dynamics modeling. A robust controller synthesis is then outlined in Section 3. Section 4 presents the robust analysis of the system and finally some conclusions and future perspectives are provided in Section 5.

## 2. BENCHMARK MODELING

The spacecraft  $\mathcal{SC}$  in Fig. 1 is composed of: the main body  $\mathcal{B}$  with its center of mass (CoM)  $B$ , its reference point  $O_b$  and its body frame  $\mathcal{R}_b(O_b; \mathbf{x}_b, \mathbf{y}_b, \mathbf{z}_b)$ ; two symmetrical flexible solar arrays  $\mathcal{A}_1$  and  $\mathcal{A}_2$  cantilevered to  $\mathcal{B}$  at the points  $P_1$  and  $P_2$  with an angular configuration  $\theta_1$  and  $\theta_2$ , respectively.  $A_i$ ,  $O_{a_i}$  and  $\mathcal{R}_{a_i}(O_{a_i}; \mathbf{x}_{a_i}, \mathbf{y}_{a_i}, \mathbf{z}_{a_i})$  are respectively the CoM, the reference point and the body frame of  $\mathcal{A}_i$  ( $i = 1, 2$ ). The angular configurations of the two solar panels are symmetrical:  $\theta_1 = \theta$  and  $\theta_2 = -\theta$ . In the Figure,  $\mathcal{R}_{a_i}(0)$  and  $\mathcal{R}_{a_i}(\theta_i)$  represent two geometric configurations of  $\mathcal{R}_{a_i}$  for the nominal configuration ( $\theta_i = 0$ ) and for a given angle  $\theta_i$ .  $[\mathbf{D}_B^{\mathcal{SC}}]_{\mathcal{R}_b}^{-1}(s, \theta)$  is the model of the spacecraft  $\mathcal{SC}$  at the CoM  $B$  of the main body  $\mathcal{B}$  and projected in the main body frame axes  $\mathcal{R}_b$  for a given angular configuration  $\theta$ , that is the  $6 \times 6$  transfer between:

- the resultant external wrench  $[\mathbf{W}_{ext/\mathcal{B}, B}]_{\mathcal{R}_b}$  (6 components: 3 forces and 3 torques) applied to  $\mathcal{B}$  at the point  $B$ ,
- the dual vector of acceleration  $[\ddot{\mathbf{x}}_B]_{\mathcal{R}_b}$  of point  $B$  (6 components: 3 translations, 3 rotations).

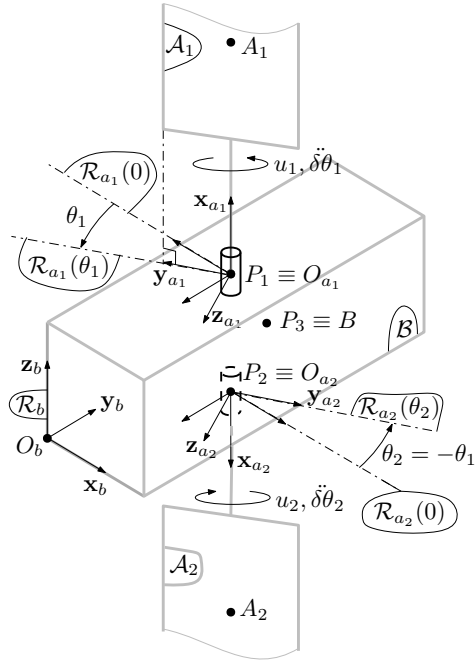


Fig. 1. Spacecraft geometry.

### 2.1 Main Body

This body can be simply modeled with the block `multi port rigid body` of the sub-library `6 dof bodies` of the SDTlib. Please refer to Table 1 for all benchmark data. The model  $[\mathbf{D}_{P_1, P_2, P_3}^{\mathcal{B}}]_{\mathcal{R}_b}^{-1}$  defines the transfer functions among the wrenches and the accelerations of the three connection points  $P_1$ ,  $P_2$  and  $P_3$  on body  $\mathcal{B}$ .

### 2.2 Direction Cosine Matrix

The Direction Cosine Matrix (DCM):

$$\mathbf{P}_{a_1(0)/b} = \begin{bmatrix} 0 & -1 & 0 \\ 0 & 0 & -1 \\ 1 & 0 & 0 \end{bmatrix} \quad (1)$$

defines the rotation:

- from the body  $\mathcal{A}_1$  frame:  $\mathcal{R}_{a_1}(0)$  in the nominal configuration ( $\theta = 0$ ),
- to the body  $\mathcal{B}$  frame:  $\mathcal{R}_b$ .

This matrix expresses the coordinates of  $\mathbf{x}_{a_1}(0)$ ,  $\mathbf{y}_{a_1}(0)$  and  $\mathbf{z}_{a_1}(0)$  in  $\mathcal{R}_b$ . In the same way:

$$\mathbf{P}_{a_2(0)/b} = \begin{bmatrix} 0 & 1 & 0 \\ 0 & 0 & -1 \\ -1 & 0 & 0 \end{bmatrix} \quad (2)$$

These DCMs, twiced  $\mathbf{P}_{a_2(0)/b}^{\times 2} = \text{blkdiag}(\mathbf{P}_{a_2(0)/b}, \mathbf{P}_{a_2(0)/b})$  (one for the translation, one for the rotation), can be modeled with the block `6x6 DCM` of the sub-library `3/6 dof DCM` of the SDTlib.

Note that the direct DCMs act on the inputs of the model  $[\mathbf{D}_{P_1, P_2, P_3}^{\mathcal{B}}]_{\mathcal{R}_b}^{-1}$  while the DCMs transposed are on the outputs of this model.

The DCM between frames  $\mathcal{R}_{a_1}(0)$  and  $\mathcal{R}_{a_1}(\theta)$  is associated to the rotation of a varying angle  $\theta$  around the axis  $\mathbf{x}_{a_1}$ :

$$\mathbf{P}_{a_1(\theta)/a_1(0)} = \mathbf{R}(\theta, \mathbf{x}_{a_1}) = \begin{bmatrix} 1 & 0 & 0 \\ 0 & \cos \theta & -\sin \theta \\ 0 & \sin \theta & \cos \theta \end{bmatrix} \quad (3)$$

In the same way:

$$\mathbf{P}_{a_2(\theta)/a_2(0)} = \mathbf{R}(\theta, -\mathbf{x}_{a_2}) \quad (4)$$

These DCMs can be modeled with the `6x6 v-u rotation` of the sub-library `3/6 dof DCM` of the SDTlib: Note that the angle  $\theta$  is declared as an uncertain parameter (`ureal`) varying between  $-\pi$  and  $\pi$ . This block uses the parameterisation  $\sigma_4 = \tan(\theta/4)$  to express the DCM as a Linear Fractional Transformation (LFT) in  $\sigma_4$ . The detail of this parametrization was firstly proposed by Dubanchet (2016).

### 2.3 Solar Arrays

The two symmetrical solar arrays can be modeled with the block `1 port flexible body` available in SDTlib. This block:

- computes the dynamic model  $[\mathbf{M}_{P_1}^{A_1}]_{\mathcal{R}_{a_1}}(s)$  of the body  $\mathcal{A}_1$  at the point  $P_1$  and projected in the body frame  $\mathcal{R}_{a_1}$ , that is the matrix transfer from the acceleration twist  $[\ddot{\mathbf{x}}_{P_1}]_{\mathcal{R}_{a_1}}$  imposed at point  $P_1$  by the main body  $\mathcal{B}$  to the reaction wrench  $[\mathbf{W}_{\mathcal{B}/\mathcal{A}_1, P_1}]_{\mathcal{R}_{a_1}}$  applied by body  $\mathcal{B}$  on the body  $\mathcal{A}_1$ ,
- and applies the action/reaction principle:

$$[\mathbf{W}_{\mathcal{A}_1/\mathcal{B}, P_1}]_{\mathcal{R}_{a_1}} = -[\mathbf{W}_{\mathcal{B}/\mathcal{A}_1, P_1}]_{\mathcal{R}_{a_1}} \quad (5)$$

Assuming the damping ratios are null ( $\xi = 0$ ), one can express the model as a  $6 \times 6$  transfer matrix:

$$\mathbf{M}_{P_1}^{A_1}(s) = \mathbf{D}_{P_1 0}^{A_1} + \sum_{j=1}^{n=3} \frac{\mathbf{l}_{j, P_1}^T \mathbf{l}_{j, P_1} \omega_j^2}{s^2 + \omega_j^2} \quad (6)$$

where  $\omega_j$  ( $j = 1, 2, 3$ ) are the frequencies of three flexible modes and  $\mathbf{l}_{j, P_1}$  is the  $1 \times 6$  modal participation factor

vector at the connection point  $P_1$  of the  $j$ -th solar array flexible mode.  $\mathbf{D}_{P_1 0}^{A_1}$  is finally the  $6 \times 6$  residual mass "rigidly" attached to the point  $P_1$ . Note that Eq. 6 is intrinsic and can be projected in any frame.

The low-frequency (DC) gain of the model  $\mathbf{M}_{P_1}^{A_1}(0)$  is always equal to the total mass matrix  $\mathbf{D}_{P_1}^{A_1}$  of the body  $A_1$  at the point  $P_1$ :

$$\mathbf{M}_{P_1}^{A_1}(0) = \mathbf{D}_{P_1}^{A_1} = \tau_{A_1 P_1}^T \underbrace{\begin{bmatrix} m^{A_1} \mathbf{I}_3 & \mathbf{0}_{3 \times 3} \\ \mathbf{0}_{3 \times 3} & \mathbf{J}_{A_1}^{A_1} \end{bmatrix}}_{\mathbf{D}_{A_1}^{A_1}} \tau_{A_1 P_1} \quad (7)$$

where  $\tau_{A_1 P_1}$  is the kinematic model between points  $A_1$  and  $P_1$ . As consequence:

$$\mathbf{D}_{P_1 0}^{A_1} = \mathbf{D}_{P_1}^{A_1} - \sum_{j=1}^{n=3} \mathbf{I}_{j, P_1}^T \mathbf{I}_{j, P_1} \quad (8)$$

Since it is possible to declare the mass  $m^{A_1}$ , the components of the inertia tensor  $\mathbf{J}_{A_1}^{A_1}$ , the 3 components of the vectors  $\overrightarrow{O_{a_1} A_1}$ ,  $\overrightarrow{O_{a_1} P_1}$  and all the components of the modal participation factors  $\mathbf{I}_{j, P_1}$  as uncertain parameters (`ureal`), the block `1 port flexible body` includes a WC analysis to check that the residual mass  $\mathbf{D}_{P_1 0}^{A_1}$  is always a definite positive matrix for any parametric configurations.

#### 2.4 Spacecraft Assembly

The assembled spacecraft model is depicted in Fig. 2, where the previously described sub-systems can be distinguished. In the same diagram the blocks  $\Delta_{\bullet}$  represent the parametric uncertainties and varying parameters of the various sub-systems in an upper LFT form:

- $\Delta_{\mathcal{B}} = \text{blkdiag}(\delta_{m^{\mathcal{B}}} \mathbf{I}_3, \delta_{xx} \mathbf{J}_{\mathcal{B}}^{\mathcal{B}}, \delta_{yy} \mathbf{J}_{\mathcal{B}}^{\mathcal{B}}, \delta_{zz} \mathbf{J}_{\mathcal{B}}^{\mathcal{B}})$  incorporates the parametric uncertainties on the mass and diagonal terms of the main body inertia matrix,
- $\Delta_{\mathcal{A}_{\bullet}} = \text{blkdiag}(\delta_{\omega_1} \mathbf{I}_4, \delta_{\omega_2} \mathbf{I}_4, \delta_{\omega_3} \mathbf{I}_4)$  incorporates the parametric uncertainty on the value of frequency of the first three modes of the solar panels,
- $\Delta_{\sigma_4} = \sigma_4 \mathbf{I}_8$  expresses the variations of the solar arrays' rotation angle.

The values of each of these uncertainties are specified in Table 1. Figure 3 shows the singular values of the  $3 \times 3$  transfer function among external torques  $[\mathbf{W}_{\text{ext}/\mathcal{B}, P_3}]_{\mathcal{R}_b}$   $\{4:6\}$  applied to the central body CoM and its angular accelerations  $[\ddot{\mathbf{x}}_{P_3}]_{\mathcal{R}_b}$   $\{4:6\}$ . Note how the system uncertainties determine a big shift of flexible mode frequencies.

### 3. CONTROL SYNTHESIS

#### 3.1 Problem statement

We consider the robust design of a 3-axis structured attitude control law to meet:

- (Req1) the pointing requirement, defined by the  $3 \times 1$  vector of Absolute Performance Error ( $\mathbf{APE} = [4 \ 4 \ 20]^T \text{pi}/180 \cdot 10^{-3} \text{ rad}$ ), in spite of low frequency orbital disturbances (characterized by the

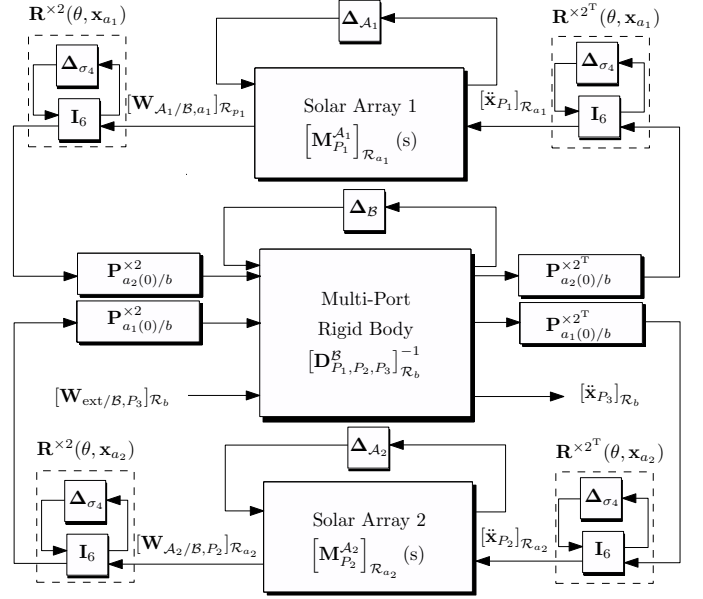


Fig. 2. Spacecraft LFT assembly.

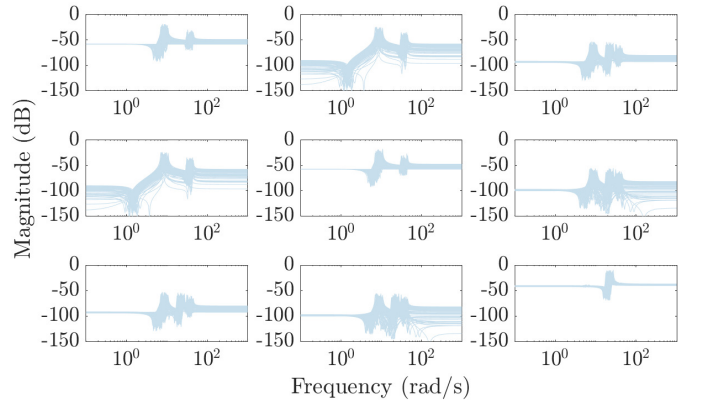


Fig. 3.  $3 \times 3$  open-loop transfer function among external torques applied to the central body CoM and its angular accelerations.

$3 \times 1$  upper bound on the magnitude  $\mathbf{T}_{\text{ext}} = [0.03 \ 0.01 \ 0.02]^T \text{ Nm}$ ,

- (Req2) stability margins characterized by an upper bound  $\gamma$  on the  $H_{\infty}$ -norm of the input sensitivity function,

while minimizing (Req3) the variance on the torque applied by the reaction wheel system on the spacecraft in response to the star sensor and gyrometer noises characterized by their Power Spectral Density (PSD), respectively  $\mathbf{PSD}^{\text{SST}} = 10^{-8} \mathbf{I}_3 \text{ rad}^2/\text{s}$  and  $\mathbf{PSD}^{\text{GYRO}} = 10^{-10} \mathbf{I}_3 \text{ rad}^2/\text{s}$  (assumed to be equal for the 3 components).

The value  $\gamma = 1.5$  ensures on each of the 3 axes:

- a disk margin  $> 1/\gamma = 0.667$ ,
- a gain margin  $> \frac{\gamma}{\gamma-1} = 3$  (9.542 dB),
- a phase margin  $> 2 \arcsin \frac{1}{2\gamma} = 38.9 \text{ deg}$ .

The requirements Req1 and Req2 must be met for any values of the uncertain mechanical parameters regrouped in the block  $\Delta = \text{blkdiag}(\Delta_{A_1}, \Delta_{\mathcal{B}}, \Delta_{A_2})$  and geometri-

System	Parameter	Description	Nominal Value	Uncertainty
Central Body $\mathcal{B}$	$m^{\mathcal{B}}$	Mass	1000 kg	$\pm 20\%$
	$[\mathbf{J}_B^{\mathcal{B}}]_{\mathcal{R}_b}$	Inertia in $\mathcal{R}_b$ frame w.r.t. $B$	$\begin{bmatrix} 75 & 1 & 2 \\ & 40 & -1 \\ sym & & 80 \end{bmatrix}$ kg m <sup>2</sup>	$\begin{bmatrix} \pm 20\% & 0 & 0 \\ & \pm 20\% & 0 \\ sym & & \pm 20\% \end{bmatrix}$
	$[\vec{O}_b \vec{B}]_{\mathcal{R}_b}$	CoM in $\mathcal{R}_b$ frame	$[0.35 \ 1.50 \ 0.50]^T$ m	–
	$[\vec{O}_b \vec{P}_1]_{\mathcal{R}_b}$	Attachment $\mathcal{A}_1$	$[0.4 \ 1.4 \ 1]^T$ m	–
	$[\vec{O}_b \vec{P}_2]_{\mathcal{R}_b}$	Attachment $\mathcal{A}_2$	$[0.4 \ 1.4 \ 0]^T$ m	–
Solar Array $\mathcal{A}_\bullet$	$m^{\mathcal{A}_\bullet}$	Mass	43 kg	–
	$[\mathbf{J}_{A_\bullet}^{\mathcal{A}_\bullet}]_{\mathcal{R}_{a_\bullet}}$	Inertia in $\mathcal{R}_{a_\bullet}$ frame w.r.t. $A_\bullet$	$\begin{bmatrix} 17 & 0 & 0 \\ & 62 & 0 \\ sym & & 80 \end{bmatrix}$ kg m <sup>2</sup>	–
	$[\vec{O}_{a_\bullet} \vec{A}_\bullet]_{\mathcal{R}_{a_\bullet}}$	$\mathcal{A}_\bullet$ CG in $\mathcal{R}_{a_\bullet}$ frame	$[2.07 \ 0 \ 0]^T$ m	–
	$[\omega_1^{\mathcal{A}_\bullet}, \omega_2^{\mathcal{A}_\bullet}, \omega_3^{\mathcal{A}_\bullet}]$	Flexible modes' frequencies	$[5.6 \ 19.3 \ 35.4]$ rad/s	$[\pm 20\% \ \pm 20\% \ \pm 20\%]$
	$[\xi_1^{\mathcal{A}_\bullet}, \xi_2^{\mathcal{A}_\bullet}, \xi_3^{\mathcal{A}_\bullet}]$	Flexible modes' damping	0.005	–
	$\mathbf{L}_{P_\bullet}^{\mathcal{A}_\bullet}$	Modal participation factors	$\begin{bmatrix} 0 & 0 & -5.12 & 0 & 12.5 & 0 \\ 0 & 0 & 0 & -3.84 & 0 & 0 \\ 0 & 0 & -2.97 & 0 & 2.51 & 0 \end{bmatrix}$ $\sqrt{\text{kg}}, \text{m} \sqrt{\text{kg}}$	–
	$\sigma_4 = \tan(\theta_\bullet/4)$	Rotor angular position	0	$[-1; 1]$

Table 1. Spacecraft data.

cal configuration  $\theta$  of the solar arrays, expressed in the uncertain block  $\Delta_{\sigma_4}^T = \text{blkdiag}(\Delta_{\sigma_4}, \Delta_{\sigma_4}, \Delta_{\sigma_4}, \Delta_{\sigma_4})$ .

Three reaction wheels connected to the central body CoM and aligned with the spacecraft reference body axes are used by the ACS. Their dynamics is modeled as a second-order low-pass filter with a natural frequency of 100 Hz and natural damping equal to 0.7:

$$\mathbf{RW}(s) = \frac{(200\pi)^2}{s^2 + 1.4 \cdot 200\pi s + (200\pi)^2} \mathbf{I}_3 \quad (9)$$

The star sensor is modeled with a first-order low-pass filter with cut-off frequency of 8 Hz:

$$\mathbf{SST}(s) = \frac{16\pi}{s + 16\pi} \mathbf{I}_3 \quad (10)$$

The gyrometer is modeled as a first-order too with a cut-off frequency of 200 Hz:

$$\mathbf{GYRO}(s) = \frac{400\pi}{s + 400\pi} \mathbf{I}_3 \quad (11)$$

The control-loop is characterized by a delay of 10 ms, that is modeled as 2nd-order Pade approximation  $\mathbf{DELAY}(s)$ .

The closed-loop generalized plant  $\mathbf{P}(s, \Delta, \Delta_{\sigma_4}^T, \mathbf{K}_{\text{ACS}}(s))$  used for the robust control synthesis is shown in Fig. 4. The LFT model of the spacecraft dynamics presented in Fig. 2 is now condensed in the upper LFT  $\mathcal{F}_u \left( [\mathbf{D}_{P_3}^{\text{SC}}]_{\mathcal{R}_b}^{-1}(s), \text{blkdiag}(\Delta, \Delta_{\sigma_4}^T) \right)$ . The following weighting filters are used to normalize the inputs and outputs:  $\mathbf{W}_{\text{ext}} = \mathbf{T}_{\text{ext}}$ ,  $\mathbf{W}_n^{\text{SST}} = \sqrt{\mathbf{PSD}^{\text{SST}}}$ ,  $\mathbf{W}_n^{\text{GYRO}} = \sqrt{\mathbf{PSD}^{\text{GYRO}}}$ ,  $\mathbf{W}_{\text{APE}} = (\text{diag}(\mathbf{APE}))^{-1}$ .

Finally the block  $\mathbf{K}_{\text{ACS}}(s)$  represents the structured  $3 \times 6$  attitude controller to be synthesized. The chosen structure is shown in Fig. 5. It is a decentralized controller composed of a proportional-derivative controller (the gains  $K_p^i$  and

$K_v^i$ ,  $i = x, y, z$ ) with a first order low pass filter (characterized by the cut-off frequency  $w^i$ ,  $i = x, y, z$ ) per axis.

The set of the 9 controller tunable parameters ( $K_p^i$ ,  $w^i$  and  $K_v^i$ ,  $i = x, y, z$ ) are roughly initialized assuming a rigid 3-axis decoupled spacecraft and in order to:

- reject a constant orbital disturbance  $\mathbf{T}_{\text{ext}}$  with a steady state pointing error  $\Theta^{\text{SC}}$  lower than the  $\mathbf{APE}(i)$  requirement on each axis  $i = x, y, z$ ,
- tune the 2-nd order closed-loop dynamics of each axis with a damping ratio  $\xi = 0.7$  and a given frequency bandwidth  $\omega^i$ .

Indeed, under these assumptions, the open-loop model between the control torque and the pointing error is equal to  $\frac{1}{\mathbf{J}_B^{\text{SC}} s^2}$ , where the nominal  $3 \times 3$  inertia  $\mathbf{J}_B^{\text{SC}}$  on the whole spacecraft at point  $B$  can be computed from the DC gain of the nominal model  $[\mathbf{D}_{P_3}^{\text{SC}}]_{\mathcal{R}_b}^{-1}(s)$ :

$$\mathbf{J}_B^{\text{SC}} = \left[ [\mathbf{D}_{P_3}^{\text{SC}}]_{\mathcal{R}_b}^{-1}(0) \right]^{-1} \{4 : 6; 4 : 6\} \quad (12)$$

Then the tuning:

$$\begin{aligned} K_p^i &= \mathbf{J}_B^{\text{SC}} \{i, i\} \omega_i^{r^2} \\ K_v^i &= 2 \xi \mathbf{J}_B^{\text{SC}} \{i, i\} \omega_i^r \end{aligned} \quad (13)$$

with  $\omega_i^r$  required bandwidth on  $i$ -th axis ( $i = 1, 2, 3$ ), ensures the needed closed-loop dynamics and a disturbance rejection function expressed as:

$$\frac{\Theta^{\text{SC}}\{i\}}{\mathbf{T}_{\text{ext}}\{i\}}(s) = \frac{1}{\mathbf{J}_B^{\text{SC}}\{i, i\}} \frac{1}{s^2 + 2 \xi \omega_i^r s + \omega_i^{r^2}} \quad (14)$$

Thus the required bandwidth  $\omega_i^r$  to meet the absolute pointing error requirement in steady state ( $\Theta^{\text{SC}}\{i\} \leq \mathbf{APE}\{i\}$ ) is:

$$\omega_i^r \geq \sqrt{\frac{\mathbf{T}_{\text{ext}}\{i\}}{\mathbf{J}_B^{\text{SC}}\{i, i\} \mathbf{APE}\{i\}}} \quad (15)$$

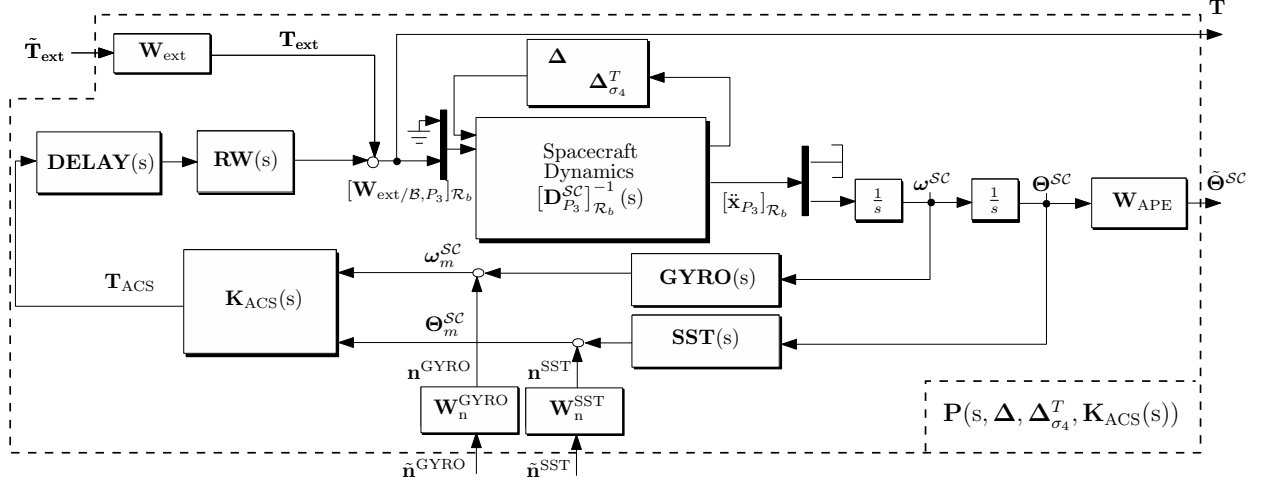


Fig. 4. Generalized plant for robust control synthesis.

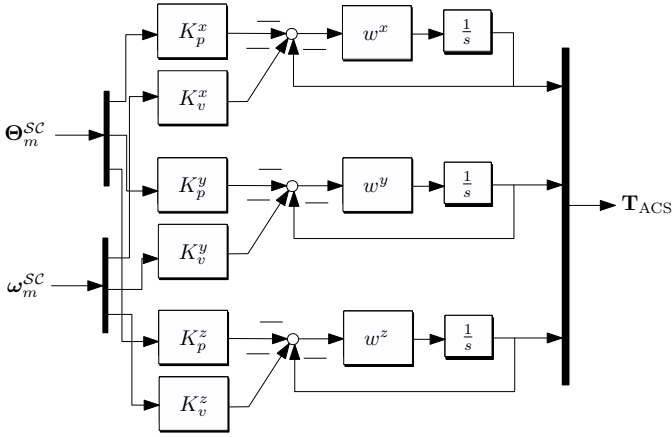


Fig. 5. Structured controller  $\mathbf{K}_{ACS}(s)$ .

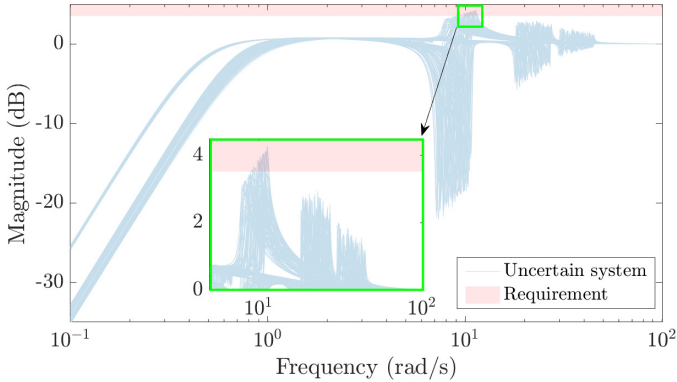


Fig. 6. Singular Values of the transfer  $\tilde{\mathbf{S}}(s, \Delta, \Delta_{\sigma_4}^T, \hat{\mathbf{K}})$  with the initial guess controller.

The frequency of the first order low pass filter  $\omega^i$  is tuned at  $20\omega_i^T$  on each axis.

This initial tuning, based on simplified assumptions (that does not verify the stability requirement (Req2) for some parametric configurations as shown in Fig. 6 and does not minimize (Req3)), is useful to initialize the non-convex optimization problem presented in the next section.

### 3.2 Robust control synthesis

In this section a robust controller is synthesized thanks to the `systeme` routine available in MATLAB, based on the non-convex optimization algorithm proposed by Apkarian et al. (2015). The three performance criteria can be easily translated into the following  $\mathcal{H}_2/\mathcal{H}_\infty$  problem. The optimization function to be optimized, that translates (Req3), is:

$$\hat{J} = \max_{\Delta, \Delta_{\sigma_4}^T} \left\| \mathbf{P}_{\tilde{\mathbf{n}} \rightarrow \mathbf{T}}(s, \Delta, \Delta_{\sigma_4}^T, \hat{\mathbf{K}}) \right\|_2 \quad (16)$$

with

$$\hat{\mathbf{K}} = \arg \min_{\mathbf{K}} \max_{\Delta, \Delta_{\sigma_4}^T} \left\| \mathbf{P}_{\tilde{\mathbf{n}} \rightarrow \mathbf{T}}(s, \Delta, \Delta_{\sigma_4}^T, \mathbf{K}) \right\|_2 \quad (17)$$

Here  $\mathbf{K}$  represents the set of 9 control parameters to be tuned;  $\left\| \mathbf{P}_{\tilde{\mathbf{n}} \rightarrow \mathbf{T}}(s, \Delta, \Delta_{\sigma_4}^T, \mathbf{K}) \right\|_2$  represents the  $\mathcal{H}_2$ -norm of the multi-input multi-output (MIMO) transfer from the normalized vector noise  $\tilde{\mathbf{n}} = [\tilde{\mathbf{n}}^{\text{GYRO}^T} \tilde{\mathbf{n}}^{\text{SST}^T}]^T$  to the control torque vector  $\mathbf{T}$  in the closed-loop generalized plant presented in Fig. 4.

The pointing requirement (Req1) corresponds to the *hard constraint* on the  $\mathcal{H}_\infty$ -norm of the MIMO transfer from the normalized external orbital perturbations  $\tilde{\mathbf{T}}_{\text{ext}}$  to normalized pointing performance  $\tilde{\Theta}$ :

$$\max_{\Delta, \Delta_{\sigma_4}^T} \left\| \mathbf{P}_{\tilde{\mathbf{T}}_{\text{ext}} \rightarrow \tilde{\Theta}}(s, \Delta, \Delta_{\sigma_4}^T, \hat{\mathbf{K}}) \right\|_\infty \leq 1 \quad (18)$$

Finally the stability requirement (Req2) on the input sensitivity function  $\tilde{\mathbf{S}}(s, \Delta, \Delta_{\sigma_4}^T, \mathbf{K}) = \mathbf{P}_{\tilde{\mathbf{T}}_{\text{ext}} \rightarrow \mathbf{T}}(s, \Delta, \Delta_{\sigma_4}^T, \mathbf{K})$  is translated into the *hard constraint* on the  $\mathcal{H}_\infty$ -norm:

$$\max_{\Delta, \Delta_{\sigma_4}^T} \left\| \tilde{\mathbf{S}}(s, \Delta, \Delta_{\sigma_4}^T, \hat{\mathbf{K}}) \right\|_\infty \leq \gamma \quad (19)$$

The WC performance indexes obtained by running `systeme` optimization are summarized in Table 2. Since all of them are lower than 1, all the control requirements are met for any parametric uncertainties and any geometric configurations according to the heuristic WC parametric and geometric configurations detected by `systeme`.

The values of the tunable parameters of the controller are detailed in Table 3. In this table the initial guess and the optimized values are compared.

WC APE	WC Stability Margins	WC Variance
0.9999	0.9999	0.1223

Table 2. Robust control synthesis WC performance indexes

	initial	optimal
$K_p^x$	429.7183	430.9168
$K_v^x$	804.2055	819.1336
$\omega^x$	14.9615	13.1309
$K_p^y$	143.2394	143.2494
$K_v^y$	463.8107	541.9954
$\omega^y$	8.6473	13.4353
$K_p^z$	57.2958	57.2995
$K_v^z$	113.6789	145.4465
$\omega^z$	14.1124	2.6361

Table 3. Controller tunable parameters: initial guess and optimal solution provided by `systune`.

#### 4. ROBUST CONTROL ANALYSIS

The last step of the end-to-end design process is the V&V campaign in order to provide a guarantee of robust stability and performance. In this section we propose some analyses run with the MATLAB routine `wcgain` of the Robust Control Toolbox and the routines available in the SMAC Toolbox developed by Biannic et al. (2016) and the STOchastic Worst-case Analysis Toolbox (STOWAT), which was first introduced by Thai et al. (2019) and Biannic et al. (2021). The analyses proposed in this articles have to be considered as simple examples while researchers are challenged to use the proposed benchmark to highlight the performance and check the limits of their own V&V algorithms.

The basis of the robust analysis is the structured singular value  $\mu$  theory presented in Zhou and Doyle (1998). Given an LFT model  $\mathcal{F}_u(\mathbf{M}(s), \Delta_M)$ , where  $\mathbf{M}(s)$  is a continuous-time stable and proper real-rational transfer function representing the nominal closed-loop system and  $\Delta_M$  is a block of uncertainties (parametric or complex), the structured singular value  $\mu$  is defined as:

$$\mu(\mathbf{M}(s)) = \frac{1}{\min_{\Delta_M} \{\bar{\sigma}(\Delta_M), \det(\mathbf{I} - \mathbf{M}(s)\Delta_M) = 0\}} \quad (20)$$

where  $\bar{\sigma}(\Delta_M)$  denotes the maximum singular values of  $\Delta_M$ . The exact computation of  $\mu(\mathbf{M}(s))$  is an NP hard problem (Braatz et al. (1994)) and several algorithms for the computation of the upper and lower bounds of  $\mu(\mathbf{M}(s))$  are available in literature.

##### 4.1 Pointing requirement

We analyze in this section the robustness of the pointing requirement (Req1). The routine `wcgain` was found to fail in the computation of the upper and lower  $\mu$  bounds due to the high number of repetitions of the parameter  $\sigma_4$  in the uncertain block  $\Delta_{\sigma_4}^T$  equal to 32. However by using the routines `mulb` and `muub` (by restricting the analysis to the frequency bandwidth  $[0, 2]$  rad/s) available in the SMAC toolbox this computation brings respectively in 2.46 s and 5.54 s to a lower bound:  $\underline{\mu}(\mathbf{P}_{\hat{\mathbf{T}}_{\text{ext}} \rightarrow \hat{\Theta}}(s, \Delta, \Delta_{\sigma_4}^T, \hat{\mathbf{K}})) =$

0.9999 and an upper bound  $\bar{\mu}(\mathbf{P}_{\hat{\mathbf{T}}_{\text{ext}} \rightarrow \hat{\Theta}}(s, \Delta, \Delta_{\sigma_4}^T, \hat{\mathbf{K}})) = 1.2092$ , which provides some conservatism due to the difference between the two bounds. Another analysis is done by sampling the parameter  $\sigma_4$  over a grid with 72 points (corresponding to every 5 degrees between  $-175^\circ$  and  $180^\circ$ ) and run the analysis by considering only the set of uncertainties  $\Delta$ . The results obtained with `wcgain` (in 302.18 s with the option LMI) and SMAC (the lower bound in 31.39 s and the upper bound with LMI option on the frequency bandwidth  $[0, 2]$  rad/s in 201.31 s) are shown in Fig. 7. The bounds are almost independent of the solar array configuration. No WC parametric configuration violating the pointing requirement was isolated (the lower bound is always under 1). On the frequency-response in Fig. 8 it can be also verified that the pointing requirement is actually saturated in low frequency for all parametric configurations.

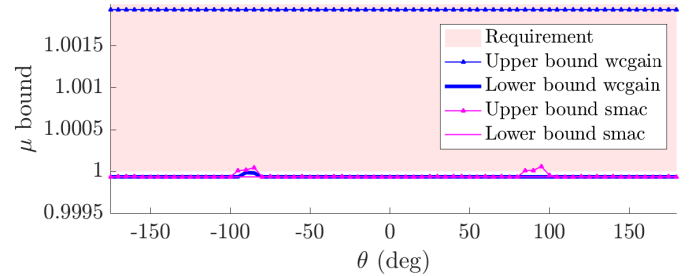


Fig. 7.  $\mu$  bounds for the pointing requirement constraint for a gridding of 72 different values of  $\sigma_4$ .

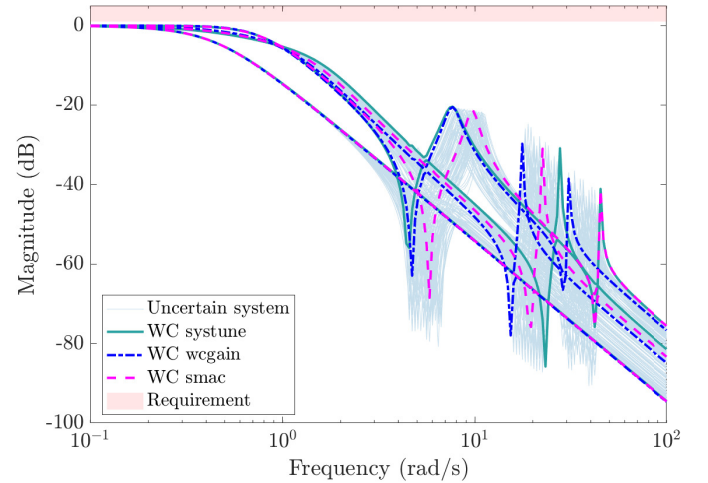


Fig. 8. Singular Values of the transfer  $\mathbf{P}_{\hat{\mathbf{T}}_{\text{ext}} \rightarrow \hat{\Theta}}(s, \Delta, \Delta_{\sigma_4}^T, \hat{\mathbf{K}})$ .

##### 4.2 Stability margin requirement

For the stability margin requirement (Req2) both `wcgain` and SMAC cannot provide the  $\mu$  upper bound if the entire set of uncertainties is considered. The same grid of  $\sigma_4$  with 72 values is then used to evaluate the  $\mu$  bounds for each sampled system. The results obtained both with `wcgain` and SMAC are shown in Fig. 9 and the computed WC are summarized in Table 4. Note that exactly the same options as for the validation of the pointing requirement are used for the two different approaches except for the

frequency range used for the computation of the upper bound with SMAC toolbox that is now  $[0, 12]$  rad/s. The following conclusions can be inferred:

- There exists some critical cases (for which  $\mu > 1.5$ ) that were not detected by `systeme` heuristic search even if the requirement is very slightly exceeded;
- Conservatism (difference between lower and upper bounds) obtained with SMAC toolbox is smaller than `wcgain`;
- The WC configuration is almost the same one for SMAC and `wcgain` and corresponds roughly to the minimum values of the inertia of the central body. This results makes physical sense since in this configuration the impact of the flexible modes of the solar panels is more important;
- The total computational cost of SMAC toolbox (lower + upper  $\mu$  bound) is  $\approx 7$  times less than the one needed by `wcgain`.

A finer grid (1001 values of  $\sigma_4$ ) is used to check better the  $\mu$  lower bound. The result is shown in Fig. 10. Following the figure a way longer analysis confirms the results obtained with the rough grid. Figure 11 shows the singular values of the sensitivity function  $\bar{\mathbf{S}}(s, \Delta, \Delta_{\sigma_4}^T, \hat{\mathbf{K}})$  with an highlight on the computed WC configurations.

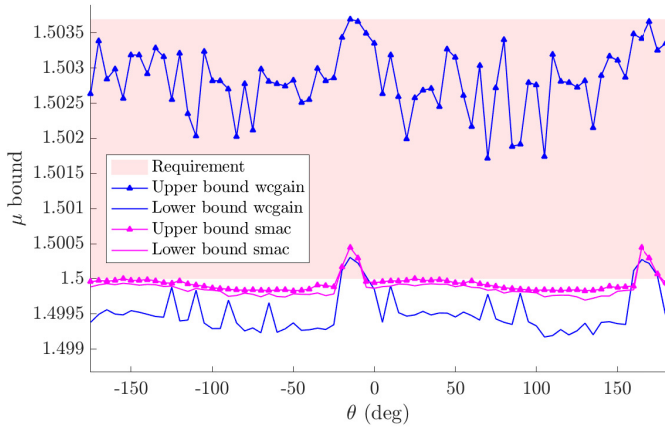


Fig. 9.  $\mu$  bounds for the stability requirement constraint for a gridding of 72 different values of  $\sigma_4$ .

For illustration of the correspondence of stability requirement with the required disk margin of  $1/\gamma = 0.667$ , Fig. 12 shows the Nichols plot obtained by opening one control axis (x,y,z) at the time.

*Probabilistic stability margin requirement* The STOWAT, is devoted to probabilistic  $\mu$ -analysis and is used in this work to perform probabilistic  $\mathcal{H}_\infty$  performance analyses, to study Req2 in more depth. The probabilistic  $\mathcal{H}_\infty$  performance algorithm of the STOWAT is limited to Single Input Single Output (SISO) system analysis. Therefore, a loop-at-a-time analysis is performed for the considered MIMO model by taking a uniform probability distribution for each uncertainty. Similar to the `wcgain` and SMAC routines, the STOWAT computations should be performed on a reduced frequency range. The robust controller is first studied on the same range as used for the SMAC routines,  $[0, 12]$  rad/s. On this domain, it can be shown that the probability of non-performance is guaranteed to

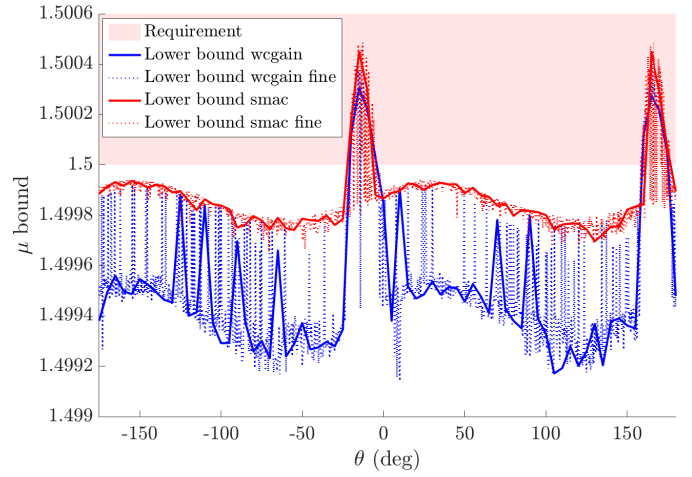


Fig. 10.  $\mu$  lower bounds for the stability requirement constraint for a gridding of 72 (solid lines) and 1001 (dotted lines) different values of  $\sigma_4$ .

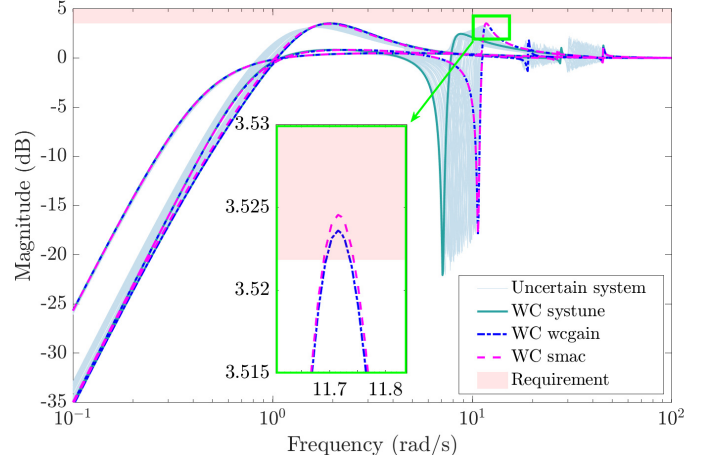


Fig. 11. Singular Values of the transfer  $\bar{\mathbf{S}}(s, \Delta, \Delta_{\sigma_4}^T, \hat{\mathbf{K}})$ .

be less than 2.5%. The total CPU time for the three SISO analyses and the preliminary stability analysis is  $\sim 37$  minutes. More accurate, lower probabilities of performance violation can be computed at the cost of an increased CPU time. Using the previously acquired knowledge of the system, regarding the WC configurations presented in Fig. 11, a more efficient analysis can be done. This by considering only a small range focused on the detected WC configurations,  $[11, 12]$  rad/s. Indeed, on this range, it can be computed in  $\sim 12$  minutes that the probability of non-performance is guaranteed to be less than 0.5% for all three considered loops. For comparative purposes, the initial guess controller is analyzed at this same narrow frequency range. As expected, this controller performs worse. The probability of non-performance is guaranteed to be higher than that of the robust controller. Even though, the probability of non-performance for the first and last SISO transfer is less than 0.5%, the probability for the second transfer indeed lies between 0.5% and 3.7%.

	WC $\mu$	WC Frequency (rad/s)	WC $\theta$ (deg)	WC Parameters							CPU Time (min)
				$m^B$ (kg)	$J_B^B\{1,1\}$ (kg m <sup>2</sup> )	$J_B^B\{2,2\}$ (kg m <sup>2</sup> )	$J_B^B\{3,3\}$ (kg m <sup>2</sup> )	$\omega_1^{A\bullet}$ (rad/s)	$\omega_2^{A\bullet}$ (rad/s)	$\omega_3^{A\bullet}$ (rad/s)	
wcgain	1.5003	11.7146	-15	814.99	60	32.82	64	6.720	15.877	42.480	48.10
SMAC	1.5004	11.7211	-15	800	60	32	67.22	6.720	22.383	42.480	6.53

Table 4. Stability margin performance WC results. CPU time accounts for lower and upper bound computation.

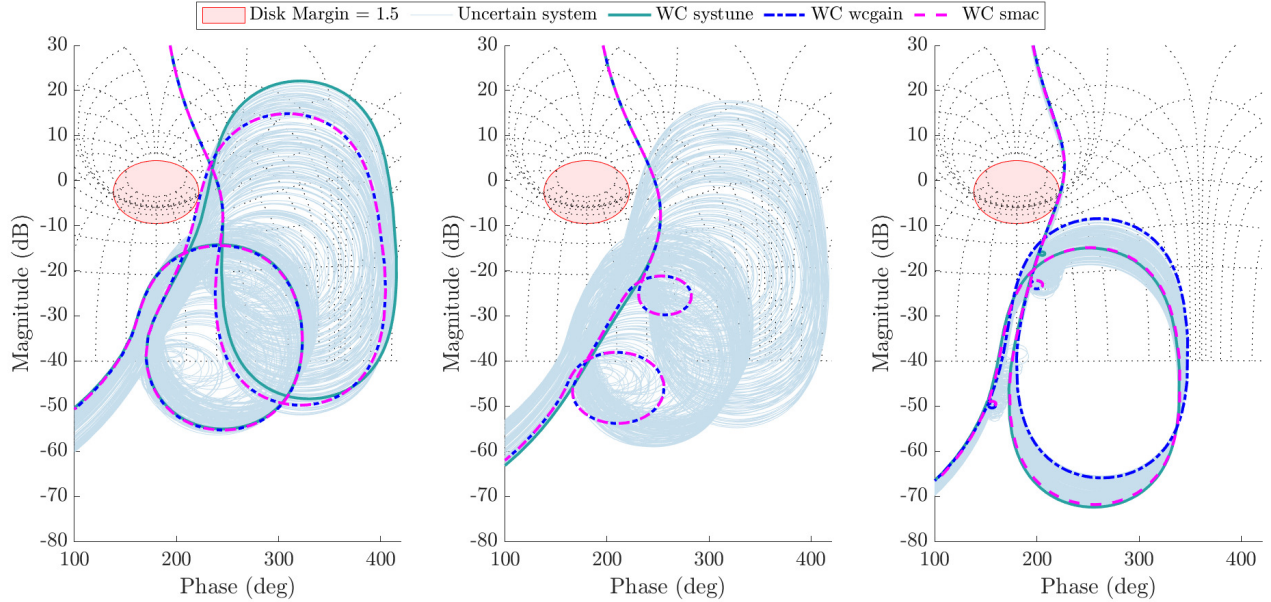


Fig. 12. Nichols plot of open-loop transfer obtained by opening one control axis (x,y,z) at the time.

### 4.3 Variance requirement

For the V&V on the variance requirement (Req3) no existing tool to the authors' knowledge is able to provide an analytically guaranteed performance.

## 5. CONCLUSION

A tutorial on modeling, robust control and analysis has been presented for the design of the attitude control system of a flexible spacecraft. The message the authors care about is that with the LFT framework offered by proper modeling, synthesis and analysis tools, as shown in this tutorial, industrial practice, largely based on simplified SISO nominal control synthesis and time-consuming Monte Carlo simulations, could benefit from these techniques to: directly obtain a robust controller, by taking into account in the model all system uncertainties from the very beginning of the control design phase; save time in V&V process by directly detect worst-case configurations in frequency domain that could escape to sampled-based Monte Carlo simulations in time domain.

## ACKNOWLEDGEMENTS

The authors thank Clément Roos (ONERA) for his advice and support.

## REFERENCES

Alazard, D., Perez, J.A., Cumer, C., and Loquen, T. (2015). Two-input two-output port model for mechanical systems. *AIAA GNC Conference*.

- Alazard, D. and Sanfedino, F. (2020). Satellite dynamics toolbox for preliminary design phase. *43rd Annual AAS Guidance and Control Conf.*, 30, 1461–1472.
- Apkarian, P., Dao, M.N., and Noll, D. (2015). Parametric robust structured control design. *IEEE Trans. on Automatic Control*, 60(7), 1857–1869.
- Balas, G., Chiang, R., Packard, A., and Safonov, M. (2021). Robust control toolbox 3 user's guide. Technical report, MATLAB.
- Biannic, J.M., Roos, C., Bennani, S., Boquet, F., Preda, V., and Girouart, B. (2021). Advanced probabilistic  $\mu$ -analysis techniques for AOCs validation. *European Journal of Control*, 62, 120–129.
- Biannic, J., Burlion, L., Demourant, F., Ferreres, G., Hardier, G., Loquen, T., and Roos, C. (2016). The smac toolbox: a collection of libraries for systems modeling, analysis and control.
- Braatz, R.P., Young, P.M., Doyle, J.C., and Morari, M. (1994). Computational complexity of/spl mu/calculation. *IEEE Trans. on Automatic Control*, 39(5), 1000–1002.
- Doyle, J. (1982). Analysis of feedback systems with structured uncertainties. 129(6), 242–250.
- Dubanchet, V. (2016). *Modeling and control of a flexible Space robot to capture a tumbling debris*. Ph.D. thesis, ISAE-SUPAERO, Polytechnique Montréal.
- Thai, S., Roos, C., and Biannic, J.M. (2019). Probabilistic  $\mu$ -analysis for stability and  $\mathcal{H}_\infty$  performance verification. In *Proceedings of the ACC*, 3099–3104.
- Zhou, K. and Doyle, J.C. (1998). *Essentials of robust control*. Prentice hall Upper Saddle River.